Extending the Lasing Wavelength Coverage of Organic Semiconductor Nanofibers by Periodic Organic–Organic Heteroepitaxy

Francesco Quochi, Günther Schwabegger, Clemens Simbrunner, Francesco Floris, Michele Saba, Andrea Mura, Helmut Sitter, and Giovanni Bongiovanni*

Organic semiconductor lasers have been the subject of vigorous research endeavors for quite a long time,[1] owing to their potential for micro-optical applications as integrated optical sources in lab-on-a-chip and compact spectroscopic systems,[2] and active chemical sensors.[3] Although laser diodes based on organic semiconductors have not been demonstrated yet, organic semiconductor lasers can effectively be pumped above the lasing threshold by inorganic semiconductor laser diodes,[4] or even light-emitting diodes,[5] a technique which has often been referred to as "indirect electrical pumping".[1]

Among the various classes of organic semiconductors, small organic molecules are very appealing for their ability to self-assemble in nanostructures upon molecular deposition on planar surfaces,[6] thereby enabling organic semiconductor lasers with applications at the nanoscale. In organic molecular films, structural and morphological disorder can lead to random laser action,[7] i.e., lasing on disorded-induced optical modes.[8] Random lasing could in fact be exploited in organic nanostructures at surfaces to achieve high-sensitivity integrated nanosensors[9] and illuminators for optical microscopy with unprecedented performances.[10]

Para-sexiphenyl (*p*6P) nanofibers represent an important example of self-assembled organic nanostructures capable of laser action.[11] Due to a favorable surface adsorption geometry,[12] vacuum deposition of *p*6P on muscovite mica leads to formation of parallel fibers whose constituent crystallites possess a well-defined contact plane and high azimuthal order. These nanofibers were proven to yield strongly polarized deep-blue emission[11] and light guidance,[13] as well as amplified spontaneous emission and random lasing.[14] Insight into the photophysics of the nanofibers revealed that bimolecular recombination, very effective in shortening the *p*6P optical gain lifetime, hinders random lasing performance under nanosecond pulsed pumping at room temperature.[15] An effective strategy to sidestep the hurdle of bimolecular recombination, hence so improving overall lasing performance, has been identified in doping the *p*6P crystals with suitable molecules, providing efficient energy sensitization via resonance-energy transfer (RET) and emission at longer wavelengths.[16]

Recently, we have demonstrated the effectiveness of organic–organic heteropitaxy on muscovite mica surfaces in fabricating *p*6P/α-sexithiophene (6T) nanofibers by means of alternated deposition of the two molecular species on *p*6P nanofiber templates. Bilayer[17] and periodic[18] heterostructures were realized with well-defined epitaxial alignment and azimuthal orientation of both *p*6P and 6T crystal phases. A materials science recipe was in fact perfected to template morphological and optical anisotropy characteristics of blue-emitting *p*6P nanofibers to materials emitting on the green and red portions of the visible spectrum. In particular, efficient *p*6P-to-6T resonance-energy transfer was shown to enable tuning of the emission color by simple variation of the thickness of the *p*6P and 6T alternated layers.[18]

In this Communication, we give proof of the great potential of organic–organic heteroepitaxy at planar surfaces by realizing 6T sensitization through RET in 6T/*p*6P nanofibers periodically grown on muscovite mica. We successfully exploit the heterostructure to (i) extend the wavelength coverage of nanofiber lasing from the deep blue to the red-orange, and (ii) suppress bimolecular recombination and, thus, achieve nanofiber laser action in the linear (or monomolecular) excited-state recombination regime. The alternated deposition approach with multiple oligomers is also envisioned as a path to nanofiber lasing with ultrahigh bandwidth.

Figure 1 illustrates the potential of temperature-controlled organic–organic heteropitaxy of *p*6P and 6T on muscovite mica. Deposition of *p*6P leads to the assembly of mutually parallel nanofibers consisting of azimuthally oriented molecular crystals. Although the combination of 6T and muscovite mica yields nanofibers with multiple orientations (Figure 1a), a *p*6P nanofiber template layer can be used to force 6T to grow on top of the *p*6P fibers (Figure 1b). Submonolayer coverages of 6T on top of *p*6P nanofibers result in the formation of a green-emitting phase of weakly interacting 6T molecules, on top of which epitaxially oriented crystals with red-orange emission nucleate for sufficiently long deposition times. The three

Dr. F. Quochi,[+] F. Floris, Dr. M. Saba,
Prof. A. Mura, Prof. G. Bongiovanni
Dipartimento di Fisica
Università di Cagliari
Complesso Universitario di Monserrato
I-09042, Monserrato-CA, Italy
E-mail: francesco.quochi@dsf.unica.it
G. Schwabegger,[+] Dr. C. Simbrunner,[+] Prof. H. Sitter
Institute of Semiconductor and Solid State Physics
Johannes Kepler University Linz
A-4040, Linz, Austria
[+]These authors contributed equally to this work.

DOI: 10.1002/adom.201200005

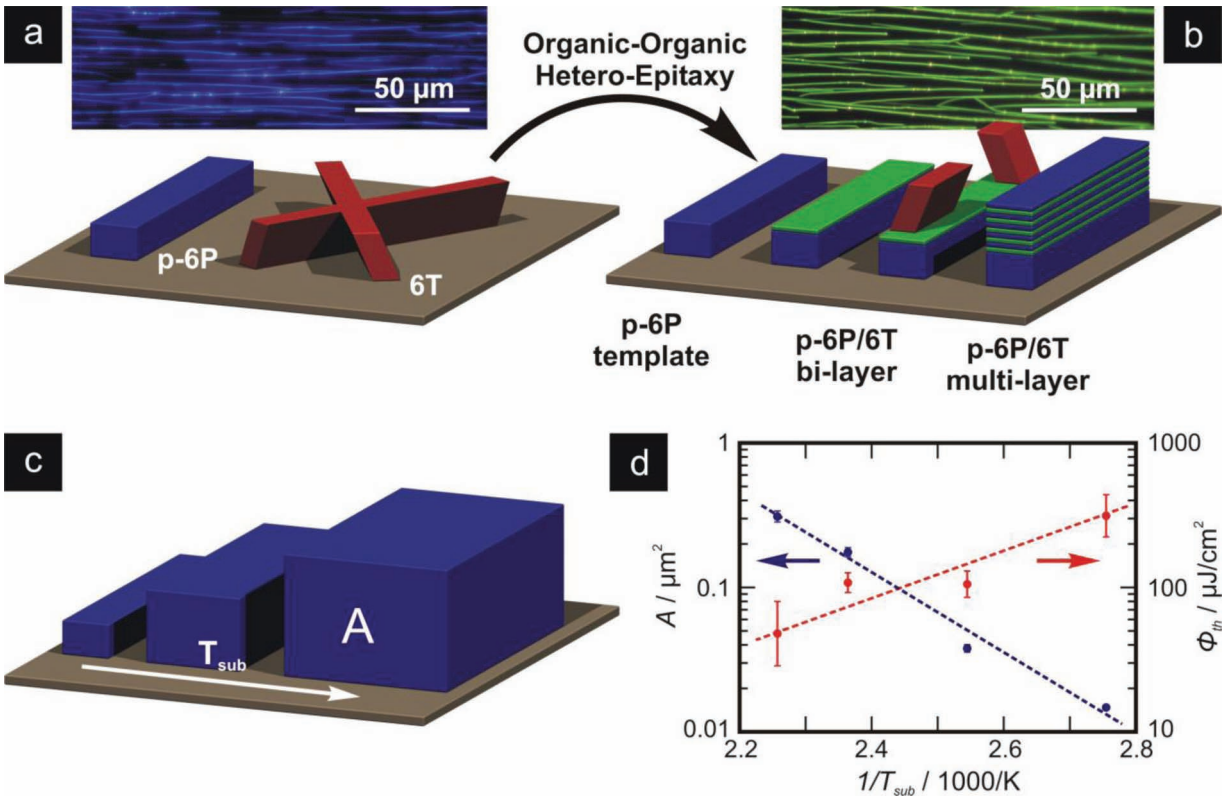

Figure 1. (a) Schematic representation of para-sexiphenyl (*p*6P) and sexithiophene (6T) nanofibers grown by vacuum deposition on muscovite mica. Sexiphenyl molecules self-assemble to yield highly oriented nanofibers, whereas deposition of sexithiophene results in fibers with multiple orientations. Top: Epifluorescence micrograph of pure p6P nanofibers is shown on top. (b) Organic (*p*6P)-organic (6T) heterepitaxy resorting to *p*6P nanofiber templates on muscovite mica allows for growing bilayer or multilayer parallel nanofibers for functional organic semiconductor nanostructures. Green layers laid over blue blocks (*p*6P crystals) represent 6T monolayers exhibiting green fluorescence, whereas red blocks on top depict red-orange emitting 6T crystallites. Top: Epifluorescence micrograph of green-emitting 6T/*p*6P nanofibers. (c) Skecth illustrating thermal activation of nanofiber dimensions: Higher substrate temperatures during deposition lead to nanofibers with larger cross-sections. (d) Dependence of cross-sectional area (*A*) and lasing threshold fluence (Φ_{th}) of pure *p*6P nanofibers (60 min deposition time) *versus* inverse substrate temperature.

material phases display parallel optical transition dipoles both in absorption and emission, thereby enabling the realization of nanofibers with broadband polarized emission.[17] By resorting to alternated deposition of *p*6P and 6T, oriented nanofibers consisting of a periodic molecular heterostructure can be obtained where the emission of 6T monolayers is efficiently sensitized by bulk *p*6P slabs via RET upon near UV photoabsorption; tuning of the nanofiber emission color can then be achieved by varying the *p*6P slab thickness.[18] In addition, fiber nucleation is a thermally activated process, so that growth temperature can be exploited to tailor the dimensions of the nanofibers as well as their photonic properties (Section II of Supporting Information). Figure 1c illustrates how the cross-section of *p*6P nanofibers, featuring lasing in the deep blue, rises with increasing substrate temperature during growth. In Figure 1d the average cross-section of *p*6P nanofibers and lasing threshold fluence under subpicosecond pumping are plotted against inverse substrate temperature, demonstrating thermal activation behaviour for the fiber cross-section. Complementary decrease of threshold fluence is evidenced, as a further demonstration that the active photonic properties of the nanofibers are intimately connected to their morphology. The observed trends could be qualitatively explained by considering that larger fiber cross-sections result in more confinement of the waveguide mode(s) of the fibers, and, therefore, in lower lasing thresholds (Section II of Supporting Information).

Heterostructure nanofibers with periodic deposition of *p*6P and 6T on *p*6P fiber templates were grown with different substrate temperatures, deposition times and number of cycles. Lasing action from 6T could be achieved in nanofiber samples grown at temperatures equal to or larger than 150 °C, so that the nanofibers could support waveguide modes at the 6T emission wavelengths up to the red-orange spectral range (Section VI of Supporting Information). Microspectroscopic characterization of individual nanofibers was undertaken with the aim at spatially resolving lasing spectra along the fibers' axes. **Figure 2** shows the lasing spectrogram of a single nanofiber excited by subpicosecond laser pulses at 392 nm slightly above the *p*6P absorption band edge so that 6T emission was sensitized through RET (the spectrogram covers the 6T emission spectral region). The fiber is part of a sample grown at 160 °C with 600 s *p*6P buffer (template) deposition time, 54 s (20 s) *p*6P (6T) deposition time per cycle for 200 cycles. Based on our calibration of growth rates (Section I of Supporting Information)

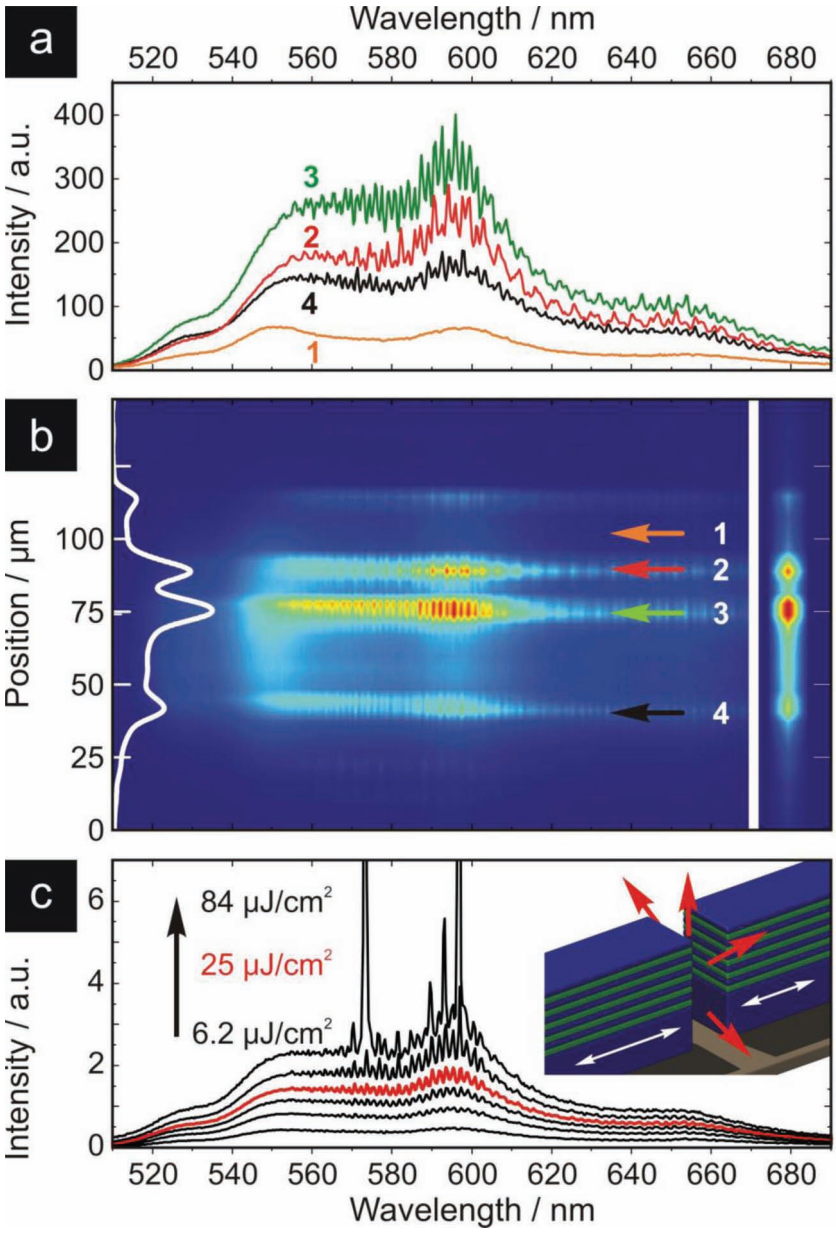

Figure 2. Laser performance of a single multilayer nanofiber grown by periodic deposition of *p*6P and 6T on muscovite mica, excited by subpicosecond pulses with 392 nm central wavelength at a pulse fluence of 25 µJ cm^{-2}. (a) Emission intensity spectra measured at different positions along the fiber axis. (b) Optical emission spectrogram acquired as a function of position along the fiber axis and emission wavelength. The emission micrograph obtained in the absence of spectral dispersion is reported on the right-hand side of the spectrogram. The white line is a smoothed spatial profile of the emission intensity. Colored arrows with numbers indicate positions along the fiber axis at which the emission intensity spectra shown in panel (a) are extracted. (c) Spatially integrated emission spectra recorded at different pump fluences: 6.2, 12, 18, 25, 42, 84 µJ cm^{-2}. The inset illustrates the process of emission scattering into out-of-plane directions acted by fiber breaks.

and assuming a surface coverage fraction of 30%, the *p*6P template fiber thickness is ~24 nm, while the *p*6P spacer and 6T layer thickesses in each cycle of the overgrown heterostructure are ~2.2 nm and 0.23 nm, respectively. The 6T layer thickess is below the monolayer limit (~0.38 nm for lying molecules),[18] hence quasi-2D islands of 6T were grown on a few monolayers of *p*6P. The optical emission spectrogram in Figure 2b highlights the presence of bright emission spots along the fiber. Previous studies revealed that bright points originate from structural cracks (fiber breaks) acting simultaneously as waveguide backreflectors for optical feedback and optical outcouplers for random lasing.[19] The emission spectra recorded at these positions (Figure 2a) display complex fringe patterns that could easily be ascribed to multipath interference realized along the fiber axes and enabled by backreflections at the breaks' positions in presence of waveguide amplified spontaneous emission. The fringes vanish for wavelengths shorter than ca. 550 nm, as a possible consequence of waveguide self-absorption. Away from the bright spots (position 1), the emission spectrum is dominated by epifluorescence, i.e., fluorescence into unguided radiation modes, and shows only vibronic peaks. Evolution of the spatially integrated emission spectrum for increasing pump fluence shows clear evidence for transition from spontaneous emission to lasing (Figure 2c). For raising pump fluence, amplified spontaneous emission progressively takes in, which is characterized by spectral fringes whose visibility increases as the fluence is raised due to progressive loss compensation by gain,[20] until lasing threshold is reached, with consequent sudden increase in slope efficiency of a subset of modes.

Comparative lasing performance under non resonant (392 nm excitation wavelength) and resonant (470 nm excitation) pumping of 6T, as well as excited-state population dynamics were investigated in ensembles of nanofibers. Data shown in **Figure 3** refer to a sample grown at 160 °C with 600 s *p*6P buffer (template) deposition time, 12 s (20 s) time per deposition cycle for *p*6P (6T) for 450 cycles. The *p*6P fiber template thickness is ~24 nm, while the *p*6P spacer and 6T layer thicknesses in each cycle of the overgrown heterostructure are ~0.49 nm and 0.23 nm, respectively, meaning that also *p*6P thickness is below the monolayer limit. 6T emission transients measured upon exciting the nanofibers near the *p*6P absorption edge at 392 nm are shown in Figure 3d. At low pump fluence, the time trace is characterized by a resolution-limited activation time and a monoexponential decay with a lifetime of ~1.3 ns. The activation dynamics of the 6T emission could be explained by considering that in the *p*6P submonolayer growth regime all *p*6P photoexcitations are surrounded by 6T acceptor molecules within a Foerster's radius distance, thereby making 6T emission sensitization a

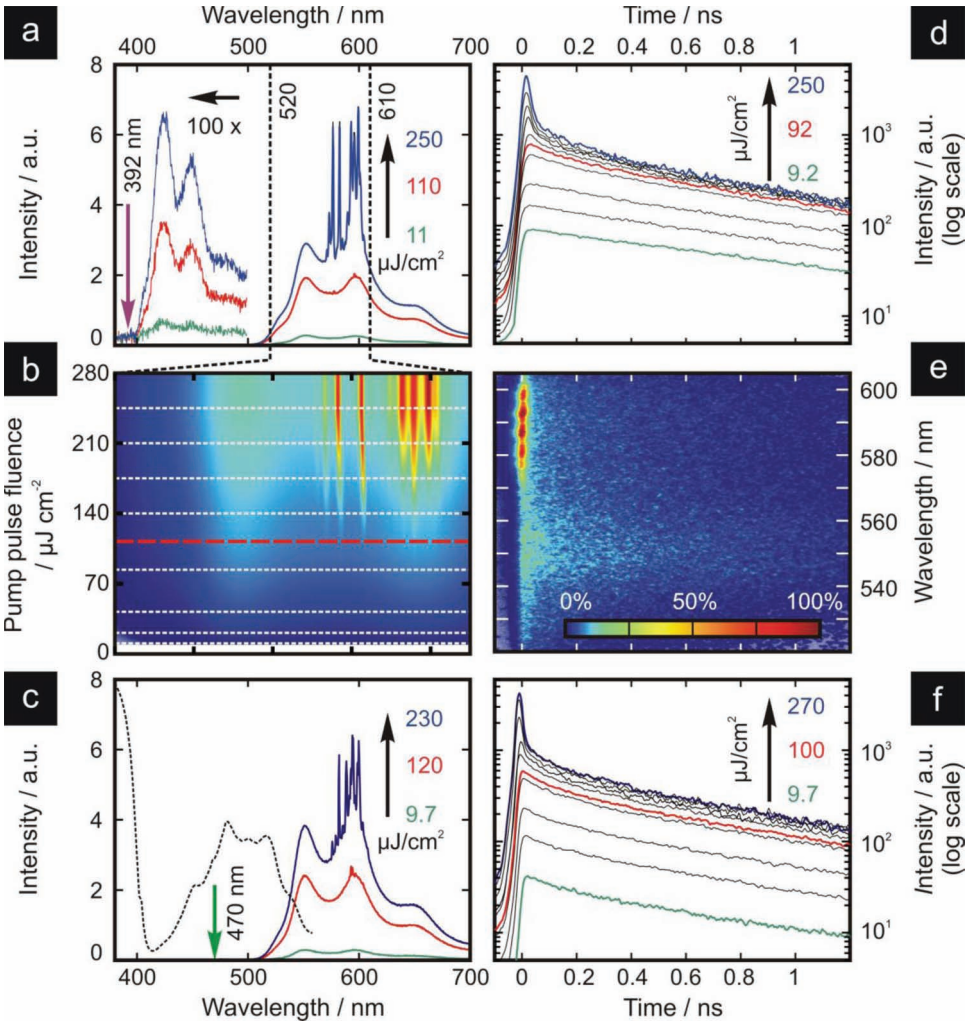

Figure 3. Laser performance of ensembles of multilayer nanofibers grown by periodic deposition of *p*6P and 6T on muscovite mica. (a) Emission spectra of nanofibers excited by subpicosecond pulses with 392 nm central wavelength (violet arrow) for various pump fluences: 11 (green), 110 (red), and 250 μJ cm^{-2} (blue curve). Intensity of the *p*6P emission is magnified 100x. (b) Spectrogram of the emission intensity as a function pump pulse fluence acquired on the expandend spectral region 520–610 nm. Dashed white lines mark the actual pump fluences used to excite the nanofibers. Dashed red line marks lasing threshold fluence. (c) Emission spectra excited at 470 nm (green arrow) at the following pump fluences: 9.7 (green), 120 (red), 230 μJ cm^{-2} (blue curve). The dashed black line is the photoluminescence excitation spectrum measured with 585–700 nm detection window. (d) Emission transients detected in 560–610 nm spectral window, excited at 392 nm for different pump fluences (bottom to top): 9.2 (green), 18, 37, 74, 92 (red), 120, 150, 180, 210, and 250 μJ cm^{-2} (blue curve). (e) Time-wavelength emission spectrogram excited at 392 nm wavelength with pump fluence of 120 μJ cm^{-2}. (f) Emission transients detected in 560–610 nm spectral window, excited at 470 nm for different pump fluences (bottom to top): 9.7 (green), 19, 39, 78, 100 (red), 130, 170, 200, 230, and 270 μJ cm^{-2} (blue curve).

very efficient process. As the pump fluence is raised, the optical emission decay time becomes faster, and, above threshold, lasing emission causes an emission burst promptly after pumping. This is reported on the time-wavelength emission intensity spectrogram reported in Figure 3e. Emission spectra recorded across the whole visible spectral range show that, owing to efficient RET, *p*6P emission is very faint (Figure 3a); above threshold, two sets of lasing modes are clearly visible on top of the 6T spectrum, one centered at 570 nm and one at 590 nm. This mode structure, detected also in single fiber measurements (Figure 2), was ascribed to simultaneous laser action on the 0–1 vibronic bands of two 6T material phases coexisting in the quasi-2D islands. In fact, the 6T emission spectrum can be seen as the superposition of the spectra of the green-emitting phase[17] and low-temperature crystal phase (Section III of Supporting Information). As the emission transient is wavelength independent across the whole 6T emission range, the excited states of two phases were inferred to be in mutual equilibrium during relaxation, adding up in the spectral domain to yield a broader bandwidth for lasing. Polarization-resolved measurements confirmed that both spontaneous emission and lasing emission from *p*6P and 6T material phases of the nanofibers are co-polarized with high (~10 dB) polarization intensity ratios (Section V of Supporting Information).[17,18]

Lasing was successfully demonstrated also for the direct excitation in the 6T absorption band at 470 nm (Figures 3c and f).

Again, emission transients show that well below threshold the decay dynamics is independent of pump fluence, whereas above threshold the prompt lasing burst quickly returns the excited state to a decay dynamics in the nanosecond time scale. The emission lifetime, as measured after the lasing burst, appears to slightly decrease with increasing pump fluence near the lasing threshold, consistent with the onset of bimolecular recombination. We point out that, upon resonant excitation, the 6T linear excited-state recombination dynamics is not monoexponential, as in fact previously reported on J-aggregates of 6T molecules on silicon dioxide.[21] Acceleration of 6T decay with pump fluence was also reported for 392-nm pumping (Figure 1d), although in that case it could in part be attributed to bimolecular recombination occurring in the *p*6P phase and making donor excited-state lifetime (and so the acceptor sensitization time) so fast that the 6T transient becomes practically indistinguishable from the impulse response measured upon direct excitation.[22]

Quantitative comparison between non resonantly (*p*6P-sensitized) and resonantly excited 6T lasing, conducted by sequentially focusing 392-nm and 470-nm pulse trains to the same spot size onto the same sample position, yielded 35 and 68 μJ cm^{-2} as the threshold fluence, respectively. The inferred 392-nm/470-nm pumping efficiency ratio is fairly consistent with the corresponding intensity ratio deduced from the photoluminescence excitation (PLE) spectrum (dashed line in Figure 3c).

Systematic measurements aimed at determining the lowest lasing threshold were performed on multiple positions of the sample using 392 nm pumping. Threshold fluences as low as 8 μJ cm^{-2}, corresponding to ~15 μJ cm^{-2} for resonant excitation at 470 nm were found. At these pump fluences, 6T recombination dynamics is independent of pump fluence, that is, monomolecular in nature. The results shown here about 6T monomolecular lasing at room temperature should be contrasted with findings in pure *p*6P epitaxial nanofibers, where monomolecular lasing was achieved only upon lattice cooling to 80 K.[14] From this finding we infer that in these *p*6P/6T heteroepitaxial nanofibers exciton diffusion and, thus, bimolecular recombination (in fact sensitive to lattice temperature) are far less effective in the 6T phases than in the *p*6P one.

Given the ~1-ns average lifetime displayed by 6T in the linear recombination regime, we project that the pump intensity necessary to reach 6T lasing threshold under slowly-varying optical excitation could be as low as ~15 kW$_p$ cm^{-2}. In turn, these values are within the reach of InGaN-based blue/green laser diodes operated in pulsed mode and focused to a submillimeter spot size.[4] Last, we shall mention that, for much higher pump intensities, we were able to observe simultaneous laser action from *p*6P and 6T on individual nanofibers (Section IV of Supporting Information).

In conclusion, we demonstrated periodic organic–organic heteroepitaxy as a powerful technique to tailor the lasing properties of organic semiconductor nanofibers. Moving from pure *p*6P epitaxial nanofibers to periodically grown *p*6P/6T heteroepitaxial nanofibers, we could successfully tune the fiber lasing wavelengths from the deep blue to the red-orange. Remarkably, monomolecular 6T lasing was achieved at room temperature. We suggest that the adopted materials growth strategy based on *p*6P/muscovite nanofiber templates could be extended to different guest oligomers for further tailoring of the lasing properties.

Experimental Section

Sample Growth: All nanofiber samples were fabricated on muscovite mica (001) substrates (SPI, Structure Probe, Inc.) by Hot-Wall Epitaxy (HWE). The growth chamber was equipped with two HWE reactors for *p*6P (TCI) and 6T (Sigma-Aldrich) deposition. The system was operated under HV conditions with a nominal pressure of ca. 10^{-5} mbar. Optimized evaporation temperature was 240 (190) °C for *p*6P (6T). The substrate was pre-heated for 30 min prior to deposition of the *p*6P buffer (fiber template). Samples were fabricated with different substrate temperatures ranging from 90 to 170 °C.

Optical Spectroscopy: Samples were optically pumped by 150-fs pulses delivered by a Ti:Sapphire regenerative amplifier (Quantronix Integra C) operating at a repetion rate of 1 kHz, focused to a circular spot with ~100 μm diameter on the organic nanofiber films. Frequency-doubled pulses centered at 392 nm wavelength were used to pump the nanofibers near the *p*6P absoption edge. An optical parametric amplifier (LightConversion Topas) was used to generate pulses at 470 nm central wavelength for direct 6T photoexcitation. The optical emission, detected in epifluorescence geometry, was collimated using a 8x objective lens (100-mm focal-length achromatic doublet) for single fiber (fiber ensemble) measurements. Individual fibers were singled out by selective imaging onto the slit aperture of the spectroscopic setup. High-resolution (<0.1 nm) optical emission spectra were measured using a 500-mm grating spectrometer (Acton SpectraPro 2500i) equipped with a liquid-N_2-cooled CCD (Princeton Instruments 7439–0001). Transient emission measurements were performed using a 300-mm spectrometer (Acton SpectraPro 2300i) coupled to a picosecond streak camera (Hamamatsu C5680) providing ~20 ps temporal resolution in operating conditions.

Photoluminescence excitation (PLE) spectra were obtained using a 450W Xe lamp monochromated with a double Czerny-Turner spectrometer (GEMINI 180) whose intensity was corrected by using Rhodamine B as a reference. PL was recorded with a SPEX 270 M monochromator equipped with a liquid-N_2-cooled CCD and the spectra were corrected for the instrument response. Epifluorescence images of the samples were obtained under UV lamp irradiation in an inverted confocal microscope (Nikon Eclipse TE2000-U).

Atomic-force microscopy (AFM) studies of the deposited nanofibers were performed using either a NT-MDT Smena or a Digital Instruments Dimension 3100 in the tapping mode.

Supporting Information

Supporting Information is available from the Wiley Online Library or from the author.

Acknowledgements

We are grateful to Dr. C. Botta for photoluminescence excitation measurements and to Anna Scheurecker for covering publication costs. Work in Cagliari was partially funded by the Regione Autonoma della Sardegna through PO-FSE Sardegna 2007–2013, L.R. 7/2007, "Progetti di ricerca di base e orientata", Project N° CRP3–114, CRP-17571, CRP-18353, CRP-24978. Work in Linz was financially supported by Land Oberösterreich project "Organische Nanostrukturen" and Austrian Science Fund (FWF): P25154-N20. CS acknowledges the "Programma Visiting Professor 2011/12" of the University of Cagliari, supported by Regione Autonoma della Sardegna (contract No. 348/21727).

Received: September 18, 2012
Revised: December 13, 2012
Published online: February 12, 2013

[1] a) I. D. W. Samuel, G. A. Turnbull, *Chem. Rev.* **2007**, *107*, 1272; b) S. Chénais, S. Forget, *Polym. Int.* **2011**, *61*, 390.
[2] C. Vannahme, S. Klinkhammer, M. B. Christiansen, A. Kolew, A. Kristensen, U. Lemmer, T. Mappes, *Opt. Express* **2010**, *18*, 24881.
[3] A. Rose, Z. Zhu, C. Madigan, T. M. Swager, V. Bulovic, *Nature* **2005**, *4347*, 876.
[4] a) T. Riedl, T. Rabe, H.-H. Johannes, W. Kowalsky, J. Wang, *Appl. Phys. Lett.* **2006**, *88*, 241116; b) A. E. Vadsekis, G. Tsimins, J.-C. Ribierre, L. O'Faolain, T. F. Krauss, G. A. Turnbull, I. D. W. Samuel, *Opt. Express* **2006**, *14*, 9211; c) H. Sakata, H. Takeuchi, *Appl. Phys. Lett.* **2008**, *92*, 113310.
[5] Y. Yang, G. A. Turnbull, I. D. Samuel, *Appl. Phys. Lett.* **2008**, *92*, 163306.
[6] H. Mizuno, I. Ohnishi, H. Yanagi, F. Sasaki, S. Hotta, *Adv. Mater.* **2012**, *24*, 2404.
[7] a) M. Anni, S. Lattante, R. Cingolani, G. Gigli, G. Barbarella, *Appl. Phys. Lett.* **2003**, *83*, 2754; b) S. Kéna-Cohen, P. N. Stavrinou, D. D. C. Bradley, S. A. Maier, *Appl. Phys. Lett.* **2011**, *99*, 041114.
[8] a) H. Cao, *J. Phys. A: Math. Gen.* **2005**, *38*, 10497; b) D. S. Wiersma, *Nature Phys.* **2008**, *4*, 359.
[9] Q. Song, S. Xiao, Z. Xu, V. M. Shalaev, Y. L. Kim, *Opt. Lett.* **2010**, *35*, 2624.
[10] B. Redding, M. A. Choma, H. Cao, *Nat. Photon.* **2012**, *6*, 355.
[11] a) H. Yanagi, T. Morikawa, *Appl. Phys. Lett.* **1999**, *75*, 187; b) A. Andreev, G. Matt, C. J. Brabec, H. Sitter, D. Badt, H. Seyringer, N. S. Sariciftci, *Adv. Mater.* **2000**, *12*, 629; c) F. Balzer, H.-G. Rubahn, *Appl. Phys. Lett.* **2001**, *79*, 3860.
[12] C. Simbrunner, D. Nabok, G. Hernandez-Sosa, M. Oehzelt, T. Djuric, R. Resel, L. Romaner, P. Puschnig, C. Ambrosch-Draxl, I. Salzmann, G. Schwabegger, I. Watzinger, H. Sitter, *J. Am. Chem. Soc.* **2011**, *133*, 3056.
[13] F. Balzer, V. G. Bordo, A. C. Simonsen, H.-G. Rubahn, *Phys. Rev. B* **2003**, *67*, 115408.
[14] F. Quochi, F. Cordella, A. Mura, G. Bongiovanni, F. Balzer, H.-G. Rubahn, *Appl. Phys. Lett.* **2006**, *88*, 041106.
[15] F. Quochi, M. Saba, F. Cordella, A. Gocalinska, R. Corpino, M. Marceddu, A. Anedda, A. Andreev, H. Sitter, N. S. Sariciftci, A. Mura, G. Bongiovanni, *Adv. Mater.* **2008**, *20*, 3017.
[16] F. Cordella, F. Quochi, M. Saba, A. Andreev, H. Sitter, N. S. Sariciftci, A. Mura, G. Bongiovanni, *Adv. Mater.* **2007**, *19*, 2252.
[17] C. Simbrunner, F. Quochi, G. Hernandez-Sosa, M. Oehzelt, R. Resel, G. Hesser, M. Arndt, M. Saba, A. Mura, G. Bongiovanni, H. Sitter, *ACS Nano* **2010**, *4*, 6244.
[18] C. Simbrunner, G. Hernandez-Sosa, F. Quochi, G. Schwabegger, C. Botta, M. Oehzelt, I. Salzmann, T. Djuric, A. Neuhold, R. Resel, M. Saba, A. Mura, G. Bongiovanni, A. Vollmer, N. Koch, H. Sitter, *ACS Nano* **2012**, *6*, 4629.
[19] F. Quochi, F. Cordella, A. Mura, G. Bongiovanni, F. Balzer, H.-G. Rubahn, *J. Phys. Chem. B* **2005**, *109*, 21690.
[20] B. W. Hakki, T. L. Paoli, *J. Appl. Phys.* **1975**, *46*, 1299.
[21] a) M. A. Loi, E. Da Como, F. Dinelli, M. Murgia, R. Zamboni, F. Biscarini, M. Muccini, *Nat. Mater.* **2005**, *4*, 81; b) E. Da Como, M. A. Loi, M. Murgia, R. Zamboni, M. Muccini, *J. Am. Chem. Soc.* **2006**, *128*, 4277.
[22] The nearly monoexponential 6T decay observed for nonresonant pumping at 392 nm was qualitatively interpreted as the convolution between the impulse decay function (obtained upon 6T resonant excitation) and the activation response function related to RET.